Wireless Magnetothermal Deep Brain Stimulation

Citation: Chen, Ritchie, Gabriela Romero, Michael G. Christiansen, Alan Mohr, and Polina Anikeeva. Wireless magnetothermal deep brain stimulation. Science 347.6229 (March 27, 2015), pp. 1477-1480.

As Published: http://dx.doi.org/10.1126/science.1261821

Publisher: American Association for the Advancement of Science (AAAS)

Persistent URL: http://hdl.handle.net/1721.1/96011

Version: Author's final manuscript: final author's manuscript post peer review, without publisher's formatting or copy editing

Wireless Magnetothermal Deep Brain Stimulation

Ritchie Chen[1,2], Gabriela Romero[2], Michael G. Christiansen[1,2], Alan Mohr[3], and Polina Anikeeva[1,2*]

[1] Department of Materials Science and Engineering, Massachusetts Institute of Technology, Cambridge, MA 02139, USA.

[2] Research Laboratory of Electronics, Massachusetts Institute of Technology, Cambridge, MA 02139, USA.

[3] Department of Chemical Engineering, Massachusetts Institute of Technology, Cambridge, MA 02139, USA.

*Correspondence to: anikeeva@mit.edu

Wireless deep brain stimulation of well-defined neuronal populations could facilitate the study of intact brain circuits and the treatment of neurological disorders. Here we demonstrate minimally-invasive and remote neural excitation through the activation of the heat-sensitive capsaicin receptor TRPV1 by magnetic nanoparticles. When exposed to alternating magnetic fields, the nanoparticles dissipate heat generated by hysteresis, triggering widespread and reversible firing of $TRPV1^+$ neurons. Wireless magnetothermal stimulation in the ventral tegmental area of mice evoked excitation in subpopulations of neurons in the targeted brain region and in structures receiving excitatory projections. The nanoparticles persisted in the brain for over a month, allowing for chronic stimulation without the need for implants and connectors.

Stimulation of deep brain structures affected by treatment-resistant psychiatric and neurological disorders can ameliorate associated symptoms but is currently only achieved by permanently implanted electrodes (*1*). Second-generation neuromodulation technologies rely on acoustic (*2*), electromagnetic induction (*3*), or optical (*4*) signals. These fields are largely absorbed and scattered by tissue and similarly require a conduit for deep brain stimulation. In contrast, low-radiofrequency alternating magnetic fields (100 kHz – 1 MHz) can penetrate into the body without significant attenuation and thus enable signal delivery into deep brain regions (*5*). Alternating magnetic fields can be converted into biological stimuli by magnetic nanoparticles (MNPs) that dissipate heat via hysteretic power loss (*6*). While MNP heating has been investigated as a cell destructive therapy in magnetic hyperthermia for fifty years (*7*), this effect has only recently been exploited for control of cell membrane depolarization and gene expression in engineered xenografts and invertebrates (*8, 9*). Magnetothermal control of neural activity *in vivo* in a mammalian system remains to be demonstrated.

To achieve reversible neuronal activation with alternating magnetic fields, we developed an intracellular calcium control scheme by sensitizing cells to heat generated from MNPs (**Fig. 1A**). Earlier experiments relied on synthetic transgenes to target MNPs to the cell membrane and required 10s to 1000s of seconds to observe increased calcium ion (Ca^{2+}) influx, which exceeded temporal dynamics of neuronal firing by orders of magnitude. Recent studies suggest that MNP functionalization with proteins induces cell internalization and the formation of protein coronas that may reduce the effectiveness of targeting and heat dissipation *in vivo (10, 11)*. We reasoned that un-targeted Fe_3O_4 MNPs optimized for efficient heat dissipation at clinically relevant alternating magnetic field conditions can (i) reduce the latency period for neural excitation, (ii) eliminate exogenous targeting transgenes, and (iii) have chronic utility *in vivo* because MNPs exhibit minimal cytotoxicity and remain intact several months after injection (*12, 13*). Spherical Fe_3O_4 MNPs 22 nm in diameter possess some of the highest heating rates per gram, or specific loss power, measured for a synthetic material at a therapeutically relevant frequency f=500 kHz and field amplitude H_o=15 kA/m (*14*). We prepared these monodisperse MNPs via the thermal decomposition of an environmentally benign iron-oleate precursor (*15*), and dispersed them in water through high-temperature ligand exchange with poly(acrylic acid) (**Fig. 1B**) (*14*). Grafting poly(ethylene glycol) chains onto poly(acrylic acid) coated MNPs resulted in their steric dispersion, which improved colloidal stability (**Fig. 1C, D**) and

biocompatibility, as indicated by the increased viability of human embryonic kidney (HEK293FT) cells over prolonged exposure (**Fig. S1**) (*16*). These MNPs exhibited specific loss power of 660 W/g ± 50, which is 6-fold higher than hyperthermia agents currently used in clinical settings (**Fig. S2**). Magnetic fields were generated by a resonant coil custom-designed for fluorescence imaging during stimulation (**Fig. S3A-E**). Although TRPV1 is naturally expressed across the mammalian nervous system (*17*), we designed a transgene to establish sustained and uniform levels of TRPV1 expression for magnetothermal membrane depolarization across different cell lines (*18*). The TRPV1 transgene was placed under the excitatory neuronal promoter calmodulin kinase II α-subunit along with mCherry separated from TRPV1 by the post-transcriptional cleavage linker p2A (*CamKIIα::TRPV1-p2A-mCherry*) (*19*) and packed into the lentiviral vector to enable long-term *in vitro* and *in vivo* neural transfection (*20*). Cells were additionally transfected with the adeno-associated virus serotype 9 (AAV9) carrying GCaMP6s under the neuronal promoter human synapsin (*hSyn::GCaMP6s*) for measurement of intracellular Ca^{2+} changes as a proxy for membrane depolarization (*21*). Functionality of the two genes was confirmed by observing increased fluorescence intensity in response to capsaicin, a TRPV1 agonist, and temperature increase above 43 °C in non-excitable HEK293FT cells (**Fig. S4A-C**).

We first demonstrated magnetothermal control of intracellular Ca^{2+} influx in HEK293FT cells. Fluorescence intensity maps indicated that only cells expressing TRPV1 ($TRPV1^+$) responded to the field stimulus (f=500kHz, H_o=15 kA/m) when incubated in MNP solutions (2 mg/mL), while cells not expressing TRPV1 ($TRPV1^-$) as well as $TRPV1^+$ and $TRPV1^-$ cells without field stimulus did not exhibit significant changes in intracellular Ca^{2+} concentration (**Fig. 1E**). Field-induced temperature increase in excess of 43 °C in MNP solutions triggered GCaMP6s fluorescence increase $\Delta F/F_0 > 50\%$ in 36.1% ± 4.3 (mean ± std) of $TRPV1^+$ cells, while only 1.7% ± 1.6 (mean ± std) of $TRPV1^-$ cells exhibited a similar response (**Fig. 1F** and **Fig. S5A-D**).

Magnetothermal membrane depolarization was sufficient to evoke trains of action potentials in primary hippocampal neurons expressing TRPV1 when exposed to 10 s field pulses at 60 s intervals. Viral transfection with *AAV9-hSyn::GCaMP6s*, which allows for fluorescence detection of single action potential events (*21*), and *Lenti-CamKIIα::TRPV1-p2A-mCherry* ($TRPV1^+$) or *Lenti-CamKIIα::mCherry* ($TRPV1^-$) yielded a co-expression efficiency of 57 % after 5 days (**Fig. 2A**). In MNP solutions (10 mg/ml), 85% ± 14 of $TRPV1^+$ neurons

exhibited synchronized firing within 5 s following stimulus, while only sporadic activity was observed in $TRPV1^-$ neurons (**Fig. 2B-H**). This implies that the temperature increase (**Fig. 2D**) in MNP solutions exposed to alternating magnetic field was sufficient to trigger TRPV1 (**Fig. 2H**), while avoiding non-specific thermal effects such as changes in membrane capacitance (**Fig. 2F**) (*22*). In the absence of MNPs, magnetic field did not induce appreciable solution heating (**Fig. 2C**), and no correlated response was observed in $TRPV1^+$ and $TRPV1^-$ neurons (**Fig. 2B, E, G**). We recorded neural activity from GCaMP6s temporal fluorescence traces (**Fig. S6A-D, Movie S1**) (*23*). Waves of Ca^{2+} spikes were repeatedly induced by field pulses only in $TRPV1^+$ neurons in the presence of MNPs (**Fig. 2I-P**). The observed 5 s latency between the field application and the onset of neural activity is 5-fold faster than previously described (*8*).

We next tested whether alternating magnetic field could activate a subpopulation of neurons in deep brain tissue in mice. Finite element modeling corroborated with temperature recordings in brain phantoms was used to predict local temperature changes in response to field stimulus (**Fig. S7**). Injections (2.5 µL) of MNP solution (100 mg/mL) delivered temperature gradients sufficient to reach the TRPV1 activation threshold within 5 s and cool back to 37 °C over 60 s cycles (**Fig. S7B-F**), thus avoiding prolonged exposure to noxious heat (**Fig. S7G**) (*24*).

With low endogenous expression of TRPV1 (*25*) and well-characterized projections (*26*), the ventral tegmental area (VTA) was an attractive deep brain target for initial demonstration of magnetothermal stimulation. Furthermore, phasic excitation in the VTA has therapeutic implications in the treatment of major depression (*27*). We sensitized excitatory neurons in the VTA to heat by lentiviral delivery of TRPV1, which was followed by MNP injection into the same region four weeks later (**Fig. 3A, B, S8A**). The anesthetized mice were exposed to the magnetic field conditions described above (**Fig. S8B, C**). Neuronal excitation was quantified by the extent of activity-dependent expression of the immediate early gene c-fos within a 250 µm vicinity of the MNP injection (**Fig. 3C-F**) (*28*). Neural activity was only triggered by magnetic field in the VTA of mice transfected with TRPV1 in the presence of MNPs, resulting in a significantly higher proportion of c-fos positive ($c\text{-}fos^+$) cells as revealed by a two-way ANOVA with a Bonferroni post-hoc test ($F_{1,13}=47.5$, $P < 0.0001$, **Fig. 3G**). Control subjects testing whether the MNP injection, heat dissipation with field stimulus, or TRPV1 expression alone can result in neural stimulation showed no significant c-fos expression (**Fig. 3C-E, G**).

Furthermore, the spatial extent of neuronal activation was largely collocated with TRPV1 expression in the VTA (**Fig. 3H, I**).

We next investigated whether neurons in the VTA can be activated 1 month after MNP injection to explore its chronic utility (**Fig. 3J-O**). We again observed increased c-fos expression in the VTA only in mice transfected with TRPV1 in the presence of MNPs and exposed to the magnetic field protocol described above (**Fig. 3J, M "ON"**; Student's t-test, $P < 0.02$). In these mice, we also found evidence of field-evoked upregulation of c-fos in the medial prefrontal cortex (mPFC, **Fig. 3K, N "ON"**; Student's t-test, $P < 0.02$) and nucleus accumbens (NAc, **Fig. 3L, O "ON"**; Student's t-test, $P < 0.002$), which are known to receive excitatory inputs from VTA neurons (*26*, *29*). In the absence of stimulation, neurons in the VTA near the MNP injection site and the neurons in the mPFC and NAc did not exhibit increased c-fos expression (**Fig. 3J-O "OFF"**).

We compared the biocompatibility of the MNP injection to a similarly sized stainless steel implant (**Fig. S9**). The interface between the MNP injection and the tissue exhibited significantly lower glial activation and macrophage accumulation, and higher proportion of neurons as compared to the steel implant 1 week and 1 month after surgery (**Fig. S9A-F**). The improved tissue compatibility can likely be attributed to the mechanically pliable nature of the MNP injection and sequestration via endocytosis (*12, 13*). No difference in neuronal or glial density was observed between brain tissue of stimulated and unstimulated mice, suggesting that the rapidly dissipated magnetothermal cycles cause minimal thermal damage to the surrounding tissue (**Fig. S9G**).

In this report, we demonstrated widespread and repeatable control of cellular signaling in non-excitable and electroactive cells using wireless magnetothermal stimulation *in vitro* and *in vivo*. Finer control over stimulation intensity to facilitate applications of this approach to problems in systems neuroscience can be achieved by further reducing the latency between field onset and evoked neural firing by developing MNPs with high specific loss powers (*30*) and by introducing heat-sensitive ion channels with lower thermal thresholds (*31*). Mechanosensitive potassium and chloride channels may serve as potential mediators of magnetothermal inhibition (*32*). While demonstrated for chronic stimulation of targeted neural circuits, this magnetothermal paradigm may be formulated to trigger thermosensitive ion channels endogenously expressed

in the peripheral nervous system (*17*), enabling wireless control in deep tissue regions that currently pose significant challenges to bioelectronic medicines (*33*).

References and Notes

1. J. S. Perlmutter, J. W. Mink, *Annu. Rev. Neurosci.* **29**, 229-257 (2006).
2. Y. Tufail *et al.*, *Neuron* **66**, 681-694 (2010).
3. V. Walsh, A. Cowey, *Nat. Rev. Neurosci.* **1**, 73-80 (2000).
4. E. S. Boyden, F. Zhang, E. Bamberg, G. Nagel, K. Deisseroth, *Nat. Neurosci.* **8**, 1263-1268 (2005).
5. J. H. Young, M. T. Wang, I. A. Brezovich, *Electron. Lett.* **16**, 358-359 (1980).
6. J. Carrey, B. Mehdaoui, M. Respaud, *J. Appl. Phys.* **109**, 083921-083917 (2011).
7. Q. A. Pankhurst, J. Connolly, S. K. Jones, J. Dobson, *J. Phys. D: Appl. Phys.* **36**, R167 (2003).
8. H. Huang, S. Delikanli, H. Zeng, D. M. Ferkey, A. Pralle, in *Nat. Nanotechnol.* (2010), vol. 5, pp. 602-606.
9. S. A. Stanley *et al.*, *Science* **336**, 604-608 (2012).
10. S. Tenzer *et al.*, *Nat. Nanotechnol.* **8**, 772-781 (2013).
11. A. Salvati *et al.*, *Nat. Nanotechnol.* **8**, 137-143 (2013).
12. F. K. H. van Landeghem *et al.*, *Biomaterials* **30**, 52-57 (2009).
13. C. Petters, E. Irrsack, M. Koch, R. Dringen, *Neurochem. Res.* **39**, 1648-1660 (2014).
14. R. Chen, M. G. Christiansen, P. Anikeeva, *ACS Nano* **7**, 8990-9000 (2013).
15. J. Park *et al.*, *Nat. Mater.* **3**, 891-895 (2004).
16. J. Xie, C. Xu, N. Kohler, Y. Hou, S. Sun, *Adv. Mater.* **19**, 3163-3166 (2007).
17. A. I. Basbaum, D. M. Bautista, G. Scherrer, D. Julius, *Cell* **139**, 267-284 (2009).
18. L. Naldini, U. Blömer, F. H. Gage, D. Trono, I. M. Verma, *Proc. Natl. Acad. Sci. U.S.A* **93**, 11382-11388 (1996).
19. J. H. Kim *et al.*, *PLoS One* **6**, e18556 (2011).
20. E. Asante-Appiah, A. M. Skalka, *Antiviral Res.* **36**, 139-156 (1997).
21. T. W. Chen *et al.*, *Nature* **499**, 295-300 (2013).
22. M. G. Shapiro, K. Homma, S. Villarreal, C. P. Richter, F. Bezanilla, *Nat Commun* **3**, 736 (2012).
23. B. F. Grewe, D. Langer, H. Kasper, B. M. Kampa, F. Helmchen, *Nat Meth* **7**, 399-405 (2010).
24. J. R. Lepock, *Int. J. Hyperther.* **19**, 252-266 (2003).
25. D. J. Cavanaugh *et al.*, *J. Neurosci.* **31**, 5067-5077 (2011).
26. L. W. Swanson, *Brain Res. Bull.* **9**, 321-353 (1982).
27. K. M. Tye *et al.*, *Nature* **493**, 537–541 (2012).
28. S. P. Hunt, A. Pini, G. Evan, *Nature*, 632-634 (1987).
29. Lisa A. Gunaydin *et al.*, *Cell* **157**, 1535-1551 (2014).
30. J. Lee *et al.*, *Nat. Nanotechnol.* **6**, 418-422 (2011).
31. E. O. Gracheva *et al.*, *Nature* **464**, 1006-1011 (2010).
32. S. Yoo, S. Hong, Y. Choi, J. H. Park, Y. Nam, *ACS Nano* **8**, 8040-8049 (2014).
33. K. Birmingham *et al.*, *Nat Rev Drug Discov* **13**, 399-400 (2014).
34. G. Paxinos, K. B. J. Franklin, *The mouse brain in stereotaxic coordinates*. Gulf Professional Publishing (2004).
35. Y. Rabin, *Int. J. Hyperther.* **18**, 194-202 (2002).
36. A. Cervadoro *et al.*, *PLoS One* **8**, e57332 (2013).
37. J. T. Leith, R. C. Miller, E. W. Gerner, M. L. M. Boone, *Cancer* **39**, 766-779 (1977).
38. M. G. White, M. Emery, D. Nonner, J. N. Barrett, *J. Neurochem.* **87**, 958-968 (2003).
39. E. M. Wassermann, *Electroencephalogr. Clin. Neurophysiol.* **108**, 1-16 (1998).
40. L. C. Kloth *et al.*, *Electricity and magnetism in biology and medicine,* F. Bersani, Ed. (Springer US, 1999), Chp. 209, pp. 875-878.
41. P. A. Hasgall, E. Neufeld, M. C. Gosselin, A. Klingenböck, N. Kuster, "ITIS Database for thermal and electromagnetic parameters of biological tissues v. 2.5" (2014).
42. A. L. Sukstanskii, D. A. Yablonskiy, *Proc. Natl. Acad. Sci. U.S.A* **103**, 12144-12149 (2006).

Acknowledgments:

We would like to thank K. Deisseroth, D. Julius, and F. Zheng for generous gifts of plasmids and cell lines, C. Ramakrishnan for molecular biology advice, the GENIE project and HHMI Janelia Farm for *AAV9-hSyn::GCaMP6s* supplied by the University of Pennsylvania vector core, and D. Irvine and A. Jasanoff for their thoughtful comments on our manuscript. This work was funded in part by DARPA Young Faculty Award (D13AP00043), the McGovern Institute for Brain Research, and the NSF CAREER award (CBET-1253890). This work made use of the MIT MRSEC Shared Experimental Facilities under award number DMR-0819762. R.C. and M.G.C. are supported by the NSF GRFP and NDSEG fellowships respectively. Methods of analysis and additional data are included in Supporting Online Material. P.A., M.G.C., and R.C. have filed a US and international patent (application PCT/US14/67866) describing magnetically-multiplexed heating of volumes, which is peripherally related to this work.

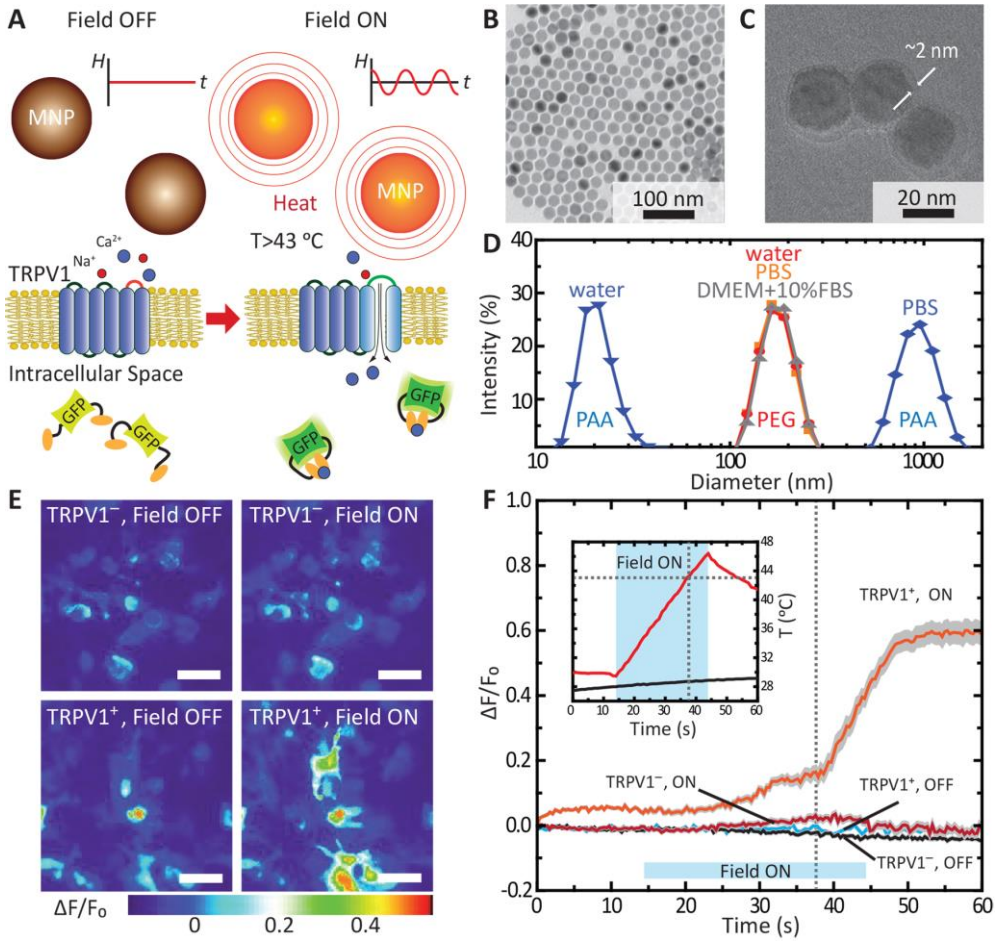

Fig. 1. Wireless ON switch for controlled magnetothermal membrane depolarization of TRPV1$^+$ cells. (A) Experimental scheme. Magnetic field stimulation ('Field ON') of TRPV1 from MNP heating is visualized by gCaMP6s fluorescence changes. **(B, C)** Transmission electron micrographs of MNPs: **(B)** as-synthesized **(C)** and after surface modification with a 2 nm poly(ethylene glycol) (PEG) shell. **(D)** Size distribution plot for poly(acrylic acid) (PAA) and PEG coated MNPs observed by dynamic light scattering. Aggregation in physiological fluids is observed for PAA coated MNPs but not for PEG coated MNPs. **(E)** Color maps of fluorescence intensity changes for TRPV1$^-$ and TRPV1$^+$ HEK293FT cells before and during magnetic field stimulus. Scale bar = 50 µm. **(F)** Normalized fluorescence intensity change ($\Delta F/F_0$) as a function of time (solid lines = mean, shaded grey areas = standard error). Dashed line corresponds to the crossing of TRPV1 activation threshold temperature. Fluorescence increase observed only in TRPV1$^+$ cells upon magnetic field application. **Inset:** Temperature profile without (gray) and with (red) magnetic field application. In all experiments field amplitude is H_o=15 kA/m and frequency is f=500 kHz.

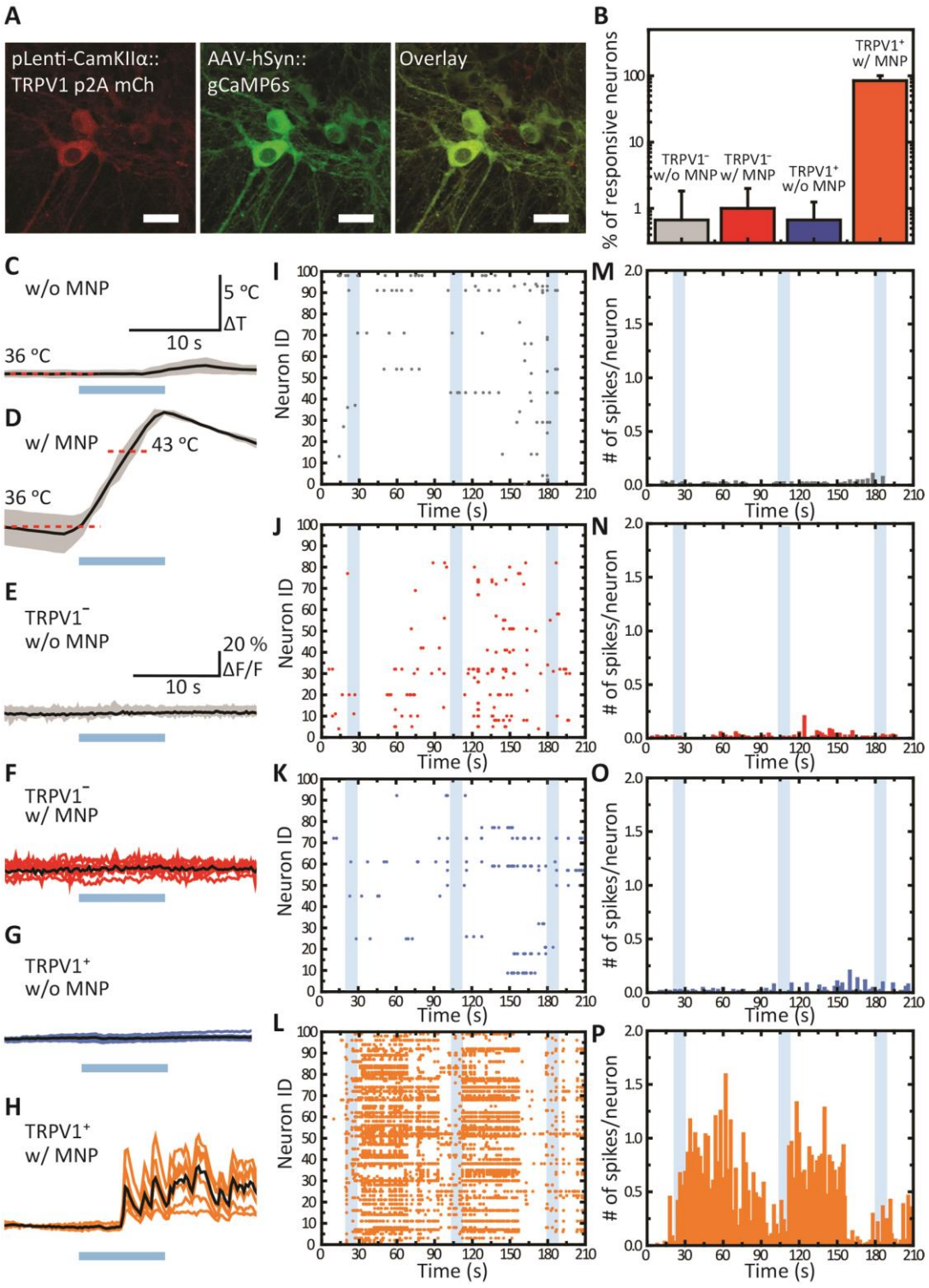

Fig. 2. Alternating magnetic field stimulus evokes correlated and repeated trains of action potentials. (A) Confocal fluorescent images of co-transfected hippocampal neurons. Scale bar = 25 μm. **(B)** Population study of 100 neurons from 3 trials counting the number of neurons that

spike within a 5 s bin following magnetic field stimulus. **(C, D)** Temperature profiles during magnetic field application in Tyrode's solution without **(C)** and with **(D)** MNPs. Shaded area is the standard deviation with average value overlaid (black). **(E-H)** Example fluorescence traces of 10 individual neurons with average overlaid (black). **(I-L)** Raster plots of 100 randomly selected neurons from 3 trials. Calcium spikes were counted according to an automated algorithm. **(M-P)** Peristimulus time histograms of the raster plots binned at 2 s. Color scheme for panels E-P: $TRPV1^-$ neurons in Tyrode's solution without MNPs (gray); $TRPV1^-$ neurons in Tyrode's solution with MNPs (red); $TRPV1^+$ neurons in Tyrode's solution without MNPs (blue); $TRPV1^+$ neurons in Tyrode's with MNPs (orange). Shaded blue bars represent alternating magnetic field pulses (H_o=15 kA/m, f=500 kHz).

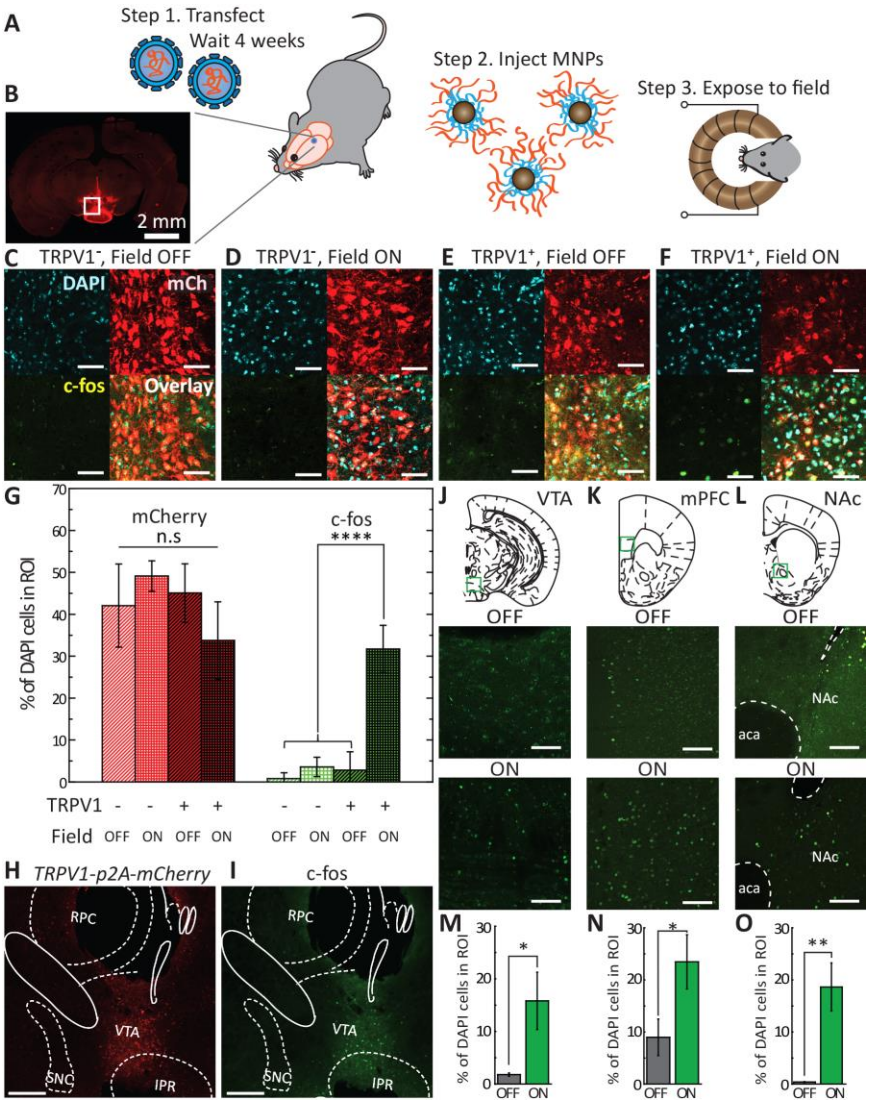

Fig. 3. Wireless magnetothermal stimulation *in vivo*. (A) *In vivo* experimental scheme. **(B)** Confocal image of a coronal slice representative of the *TRPV1-p2A-mCherry* expression profile in the VTA. **(C-F)** DAPI (cyan), mCherry (red), and c-fos (green) and overlay confocal images of regions used for quantification of neural stimulation. Scale bar = 25 μm. All animals were injected with MNPs. Experimental conditions were **(C)** without (OFF) and **(D)** with (ON) magnetic field stimulation in TRPV1^{-} VTA, and **(E)** OFF and **(F)** ON stimulation in TRPV1^{+} VTA. **(G)** Percentage of mCherry-positive and c-fos-positive neurons within cell population indicated by DAPI corresponding to the four conditions presented in **C-F**. Significance is confirmed by two-way ANOVA with Bonferroni post-hoc test (n=4, $F_{1,13}$=47.5, P < 0.0001). **(H, I)** Confocal images of the VTA after acute magnetothermal stimulation. C-fos expression is largely confined to the VTA in regions where TRPV1 is expressed. Scale bar = 100 μm. **(J-L)**

Confocal images of the (J) VTA, (K) mPFC, and (L) NAc 1 month following MNP injection without (OFF) and with (ON) field treatment. Scale bar = 100 μm. (M) Percentage of c-fos+ neurons in the VTA among DAPI-labeled cells with and without magnetic field stimulation. Increased c-fos expression is observed following field treatment (ON) as compared to unstimulated (OFF) controls (n=3 OFF/ON; Student's t-test, $P < 0.02$). (N, O) Similarly, upregulation is observed in (N) the mPFC and (O) in the NAc with alternating magnetic field (ON) as compared to the same regions without (OFF) the field stimulus (n=3 OFF/ON; Student's t- test * $P< 0.02$, ** $P < 0.002$).

Supplementary Materials:

Materials and Methods
Supplementary Text
Figs. S1-S9
Tables S1-S2
Movie S1
References (34-42)